Self-assembled UV photodetector made by direct epitaxial GaN growth on graphene

*Timotée Journot**[1,2], Vincent Bouchiat[1,3], Bruno Gayral[1,4], Jean Dijon[1,5] and Bérangère Hyot[1,2]*

1-Univ. Grenoble Alpes, 38000 Grenoble, France.
2-CEA, LETI, MINATEC campus, 38000 Grenoble, France.
3-CNRS-Grenoble, Institut Néel, 38000 Grenoble, France.
4-CEA, INAC-PHELIQS, 38000 Grenoble, France.
5-CEA, LITEN, MINATEC campus 38000 Grenoble, France.
* Corresponding author: timotee.journot@cea.fr

ABSTRACT

Hybrid systems based on the combination of crystalline bulk semiconductors with 2D crystals are identified as promising heterogeneous structures for new optoelectronic applications[1]. However, the very attractive direct integration of III-V semiconductors on 2D materials to make practical devices remains a challenge to preserve the intrinsic properties of the underlying 2D materials. In this work, we study the direct epitaxy of self-organized GaN crystals on graphene. We demonstrate that the severe MOCVD growth conditions of GaN (chemically aggressive precursors and high temperature) are not detrimental to the structural quality and the charge carrier mobility of the graphene base plane. Graphene can be so used both as an efficient sensitive material and as a substrate for GaN epitaxy to make a self-assembled UV photodetector. A responsivity as high as 2 $A \cdot W^{-1}$ is measured in the UV-A range without any further post-processing than simple deposition of contact electrodes. Our study opens the way to build new self-assembled 2D/III-V hybrid optoelectronic devices by direct epitaxy.

KEYWORDS: Graphene, gallium nitride, GaN, UV photodetector, MOCVD

Introduction

Two-dimensional (2D) materials and their combination with other types of low-dimensional materials into hybrid systems open new ways to conceive optoelectronic and photodetection devices[2]. These materials seem to be particularly interesting for sensing applications[1]. Indeed conducting 2D materials, due to their lack of bulk, are extremely sensitive to any electrostatic perturbation in their neighborhood. Thanks to its high carrier mobility, high stability and easy fabrication, graphene offers an adequate platform for photodetection. However weak light absorption in this ultrathin material limits the responsivity of purely graphene-based photodetectors[3–6]. A promising approach to enhance the photodetection sensitivity of graphene-based detectors is to combine graphene with molecules or materials that would bring to the device their optical properties. The wide band gap of Gallium Nitride (GaN) material makes it highly efficient for UV-A, B and C absorption[3]. Although purely III-Nitrides based photodetectors has already been demonstrated using thin films[7] or nanostructures[8,9]. Therefore the combination of GaN with graphene is a new way to develop high gain UV photodetectors by taking full advantage of the two systems.

The idea to hybridize graphene with another material has already been investigated. Detailed experimental studies have been reported for pentacene/graphene[10] and semiconductor (ZnO[11,12] and PbS[13,14]) quantum dots (QDs)/graphene structures. PbS QDs were used to enhance the graphene photodetection sensitivity in the infrared[13,14]. Konstantatos et al. used a mechanically exfoliated graphene surface on which PbS QDs were deposited. Upon illumination by infrared light, photoexcited holes created in PbS QDs are transferred to graphene whereas electrons are trapped in PbS due to the built-in field at the interface. Due to the long trapped-charge lifetimes in the QDs, holes recirculate many times in the graphene before they recombine. This mechanism leads to a very high photoconductive gain (10^8 electrons per photon). Thanks to this architecture Konstantatos and coworkers demonstrated the potential of hybridized graphene structures for high gain photogating detection. ZnO QDs combined with graphene have also been used as

an efficient structure sensitive in the UV spectral range[11,12]. However semiconductor QD deposition seems to be critical and the nature of chemical ligands is a key issue for the performances of the final device[13]. When QDs are deposited or assembled via chemical means, the interface between QDs and graphene is not properly controlled. However this interface is actually the active zone of the device where the charge to current conversion occurs through electrostatic doping. Therefore a precise control of the graphene/adsorbate interface is crucial. Here we show that direct growth of semiconductors on graphene is a promising method to address this issue. Indeed graphene has already been successfully studied as a growth substrate for van der Waals epitaxy of GaN nanowires[15–17] and thin film[18]. While GaN structures directly grown on graphene certainly offer a well-controlled interface, it was not obvious whether the growth conditions would be detrimental to the large-scale graphene structural quality and impact the charge carrier mobility of the graphene base plane.

In this article, we present a direct growth method of GaN crystals by MOCVD on a graphene-on-sapphire substrate. We prove that the aggressive growth conditions required to grow GaN are not detrimental to the structural quality of graphene base plane preserving the intrinsically high charge carrier mobility. Thus we show that graphene can be used both as a charge-sensitive electronic material and as an epitaxy substrate without compromise. Hence we demonstrate the 2 $A \cdot W^{-1}$ responsivity of the UV photodetector built by the as grown structure (GaN on graphene) without any post-processing beyond deposition of contact electrodes. This proof of concept attests the feasibility to preserve enough the electronic properties of graphene during the epitaxial process to then use it as an active material.

Results and discussion

Graphene is grown on Cu foil by chemical vapor deposition (CVD)[19] and then transferred onto a sapphire substrate for subsequent MOCVD growth of GaN. The high thermal stability of sapphire allows it to withstand the GaN growth conditions and its insulating character makes it possible to measure electronic transport in graphene. Trimethylgallium (TMGa) and ammonia (NH_3) act as precursors for gallium and

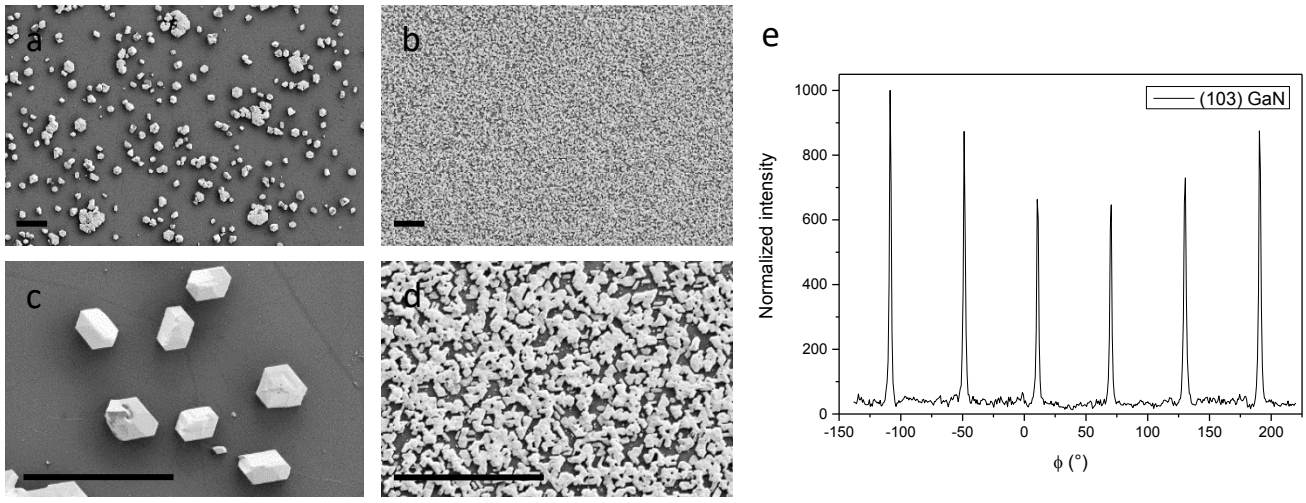

Figure 1. Top view SEM images of GaN grown on graphene ((a) and (c)) and GaN grown on sapphire ((b) and (d)) with the same growth conditions. Scale bars: 5 µm. (e) XRD φ-scan of the (103) peak of the GaN grown on graphene. The six peaks shown every 60° highlight that GaN microstructures are all crystals grown on the same direction.

nitrogen respectively[20]. The nucleation conditions of GaN on graphene are highly different from the traditionally low temperature nucleation layer used to grow GaN on sapphire[21]. In this work, a high temperature nucleation (~ 950 °C) is needed to initiate the growth of crystalline seeds. This step is nonetheless compatible with every commercial MOCVD systems. These harsh conditions have to be balanced to preserve graphene properties, more particularly its high carrier mobility. Figure 1a and Figure 1c show SEM images of the GaN microstructures grown on graphene. Seeds have a distribution in size and in density different from those grown directly on sapphire as can be seen in Figure 1b and Figure 1d. The seed density is lower with larger typical dimensions of about 2 microns in width and 500 nm in height. These features were already noted by Mun et al.[14]. As graphene is a 2D material, there are no dangling bonds on its surface and its low surface energy (~ 50 $mJ \cdot m^{-2}$ for graphene[22] and ~ 5 $J \cdot m^{-2}$ for sapphire [23]) strongly impedes the nucleation process of GaN, resulting in a lower density of microstructures than that on sapphire. The low migration energies of Ga adatoms on the graphene surface (about 30 meV according to the calculations[24]) may favor the formation of nucleation sites by self-catalyzed growth via migration and incorporation of pre-deposited Ga on the graphene.

Seeds grown on graphene show regular hexagonal shapes with sharp edges. GaN nuclei also appear to be well oriented along the c-axis normal to the substrate surface. The six fold symmetry shown on the Figure

1e proves that the GaN crystals are properly in-plane aligned. The GaN growth seems thus governed by an epitaxial relationship. Kumaresan et al. showed that graphene governs the GaN orientation when using an amorphous substrate of silica underlying graphene[15]. In our case, polycrystalline graphene (with about 20 microns wide crystals) is transferred onto a monocrystalline substrate of sapphire. This substrate seems to play an important role. Indeed the weak van der Waals interactions that control the graphene/GaN interface are long range field relative to the graphene thickness. Hence the sapphire crystalline field could contribute to the GaN seeds orientation. As previously discussed all GaN seeds grown on the whole graphene substrate have the same in-plane orientation (Figure 1a and Figure 1e) regardless of the graphene grains size. Furthermore GaN grown directly on sapphire or on graphene both have the same in-plane orientation. The sapphire crystalline field seems thus to be dominant compared to that of the graphene layer for GaN epitaxy. These observations are consistent with the work of Kim et al.[25] showing that the weak van der Waals potential of graphene cannot completely screen the stronger potential field of its underlying crystalline substrate. Hence in the sapphire/graphene/GaN structure the crystalline field of sapphire seems to control the in-plane orientation of the GaN seeds which grow above the graphene layer.

A key question in our study is whether the graphene can withstand the severe MOCVD growth conditions of GaN. Raman spectra in Figure 2a show the graphene's responses before and after GaN growth. Both spectra exhibit the three D, G and 2D characteristic Raman modes (respectively around 1350, 1590, 2700 cm^{-1}) of graphene revealing its persistence after the MOCVD growth. Some changes can be noted by looking at the Raman spectra more precisely. The full width half maximum (FWHM) of the 2D peak (Γ_{2D}) is a good indicator of the electronic conductivity of the graphene sheet[18]. Γ_{2D} is not strongly sensitive to global strain, doping and charge inhomogeneities but is strongly dependent on the electronic mobility of the graphene sheet[26]. The higher the mobility is, the lower the 2D peak FWHM is. After GaN growth, Γ_{2D} rises from 30 cm^{-1} to 38 cm^{-1}, revealing a slight reduction of the graphene mobility. This result is also consistent with the sheet resistance (R_s) measurements performed on the graphene before and after the growth; R_s increases from 5.10^3 Ω/□ to 1.10^4 Ω/□. The broadening of the G peak together with the slight

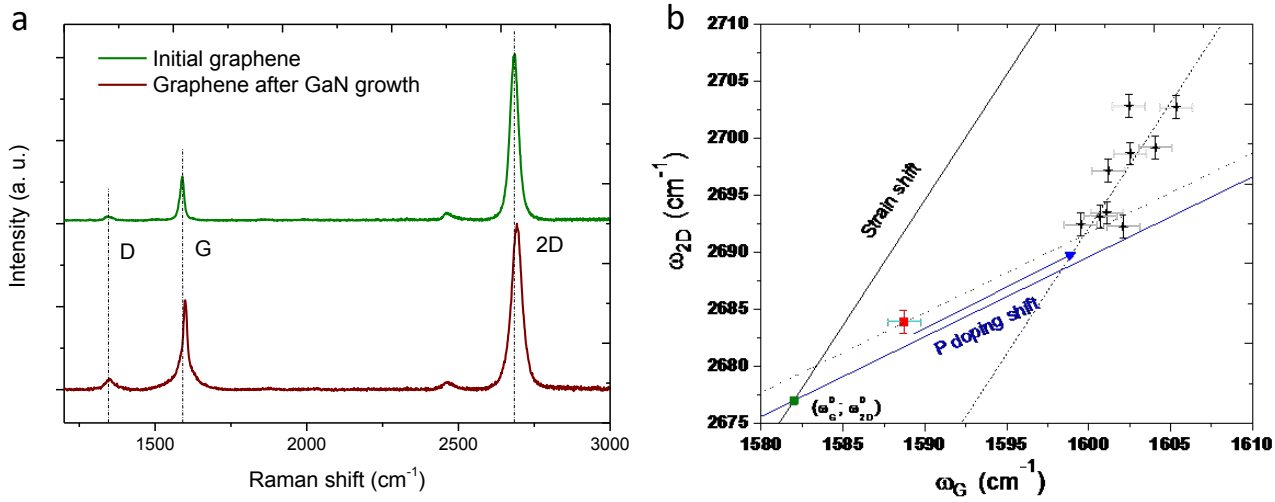

Figure 2. (a) Raman spectra of graphene before and after GaN growth (between GaN nuclei). (b) The ω_{2D} *vs* ω_G space is useful to get information on doping level and strain state of graphene. The green square ($\omega_G^0 = 1582\ cm^{-1}; \omega_{2D}^0 = 2677\ cm^{-1}$) is the position of an unstrained and undoped graphene according to Lee and Froehlicher[27,28]. The red square corresponds to the graphene transferred onto sapphire used as a template for the GaN growth. Black crosses show the response of different places on the substrate after GaN growth. Black (blue) guidelines give the 2D and G modes shifts due to strain (p doping).

increase of the D peak intensity (I_D/I_G ratio rises from 9% to 24%) during the MOCVD process reveals a slight degradation of the structural quality of graphene probably due to formation of defects caused by the exposure to ammonia atmosphere at high temperature. These structural changes may explain the doubling of the measured sheet resistance R_s after growth. In the end it should be emphasized that the graphene underlying the GaN microstructures is still of good quality in terms of electronic properties for use as a sensitive material. Raman spectra can also reveal the stress state and the doping level of the graphene layer. The frequencies of the G and 2D modes are highly sensitive to the strain state and the doping level. As the ratios $\left(\frac{\Delta\omega_{2D}}{\Delta\omega_G}\right)_{strain}$ and $\left(\frac{\Delta\omega_{2D}}{\Delta\omega_G}\right)_{doping}$ are different for the two contributions[27,28], strain and doping level can be deduced according to the Raman shifts of the G and 2D peaks. To get quantitative values, reference data of the two modes (ω_G^0 and ω_{2D}^0) for a stress free and excess charge free graphene are needed. We chose the values given by Lee et al.[27] ($\omega_G^0 = 1582$ cm^{-1}; $\omega_{2D}^0 = 2677$ cm^{-1}) acquired from freestanding graphene suspended across a circular well. These values are also in perfect agreement with references given by other teams[28,29]. By plotting on the Raman characteristics of the graphene after transfer onto sapphire and post GaN growth in the ω_G *vs* ω_{2D} space (Figure 2b), we can propose an understanding of the graphene evolution during the MOCVD growth process. Graphene used as a template

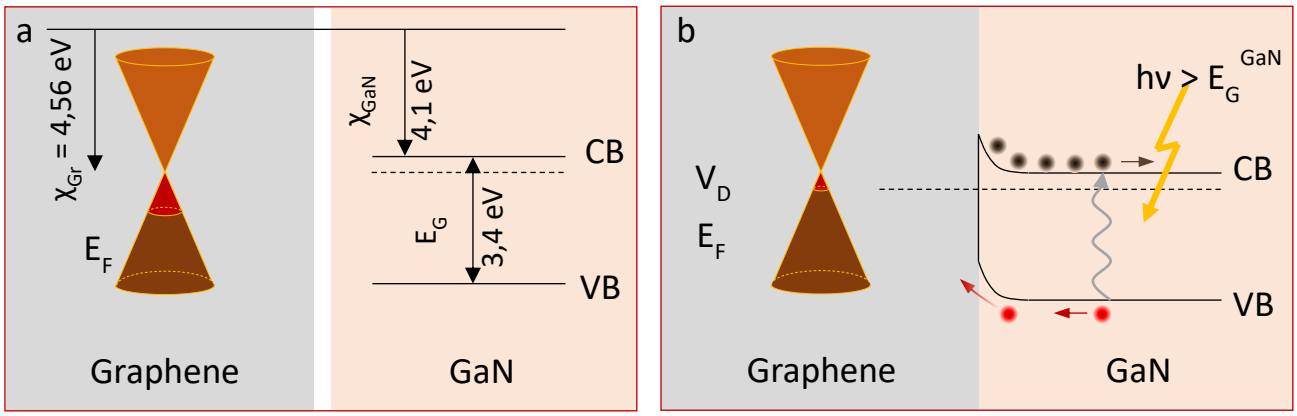

Figure 3. Schematic diagrams of energy levels showing respectively the graphene and GaN structures before (a) and after (b) contact between the two materials. A built-in field is formed at the interface (b). Under UV light illumination the created electron-hole pairs separate due to the band bending at the interface. Holes are transferred to graphene whereas electrons get trapped in GaN.

for GaN growth (red dot in the Figure 2b) is p doped and under a slightly compressive strain state. The black crosses in Figure 2b acquired after the MOCVD process indicate an increase of the p doping level. This doping level seems fairly constant across the whole sample for the nine analyzed spots. However the graphene strain state seems to be quite inhomogeneous after the growth of the GaN seeds; the black crosses are somewhat dispersed along the black dotted line which is a guideline to visualize the compressive strain effect at a constant p doping level. Using measured values of the G and 2D modes frequencies we can estimate the doping level of graphene[27,28,30]. After transfer onto sapphire, graphene is p-doped with a doping density of $5 \cdot 10^{12}$ cm^{-2}. After the GaN growth process its p doped level increases to $1.5 \cdot 10^{13}$ cm^{-2}. The adsorption of nitrogen-containing radicals on graphene must be responsible of this magnitude of the carrier concentration change[31,32]. This could also explain the slight D peak raise in the Raman spectrum of graphene measured after the GaN growth process. The Fermi energy of graphene changes accordingly as:

$$E_F(n) = \chi_{Gr} - sign(n) \cdot \hbar \cdot v_F \cdot \sqrt{\pi \cdot |n|}$$

where χ_{Gr}=4.56 eV is the graphene work function[33,34], v_F= 1.1 x 10^6 m.s^{-1}, the Fermi velocity[30,35] and n the doping density. Thus after exposure to the MOCVD precursors needed for the GaN growth, the Fermi level of graphene can be estimated at $E_F^{Gr} \approx 5.06$ eV. This value has to be compared to the Fermi level of

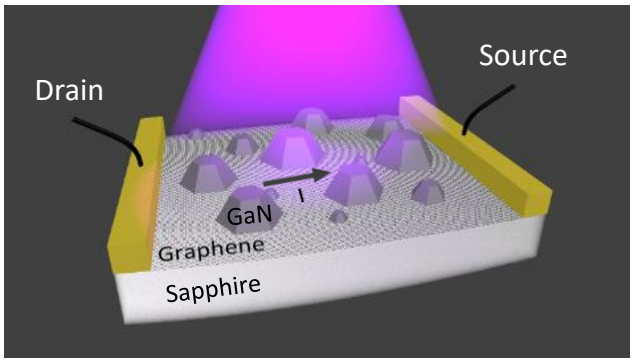

Figure 4. Schematic representation of our device.

the GaN crystals. Non-intentionally doped (nid) GaN may have residual doping levels ranging from n=10^8 to 10^{16} cm^{-3} which correspond respectively to a Fermi level of E_F^{GaN}= 4.94 and 4.46 eV. Therefore whatever the doping level of the nid GaN grown on graphene, the Fermi level of graphene is deeper than that of GaN as shown in Figure 3a. Thus when both materials are put into contact, the GaN band structure bends according to the diagram of Figure 3b due to carrier transfers at the interface. As a consequence, under illumination from a UV light source (with photon energies above the band gap of GaN), the GaN on graphene heterostructure shows a photogating effect. Photogenerated electron-hole pairs in the GaN islands are separated due to the built-in field at the interface. Holes are transferred to graphene whereas electrons get trapped in GaN (as shown on Figure 3b) from where they modulate the Fermi level and thus the conductivity of the graphene carrier transport channel.

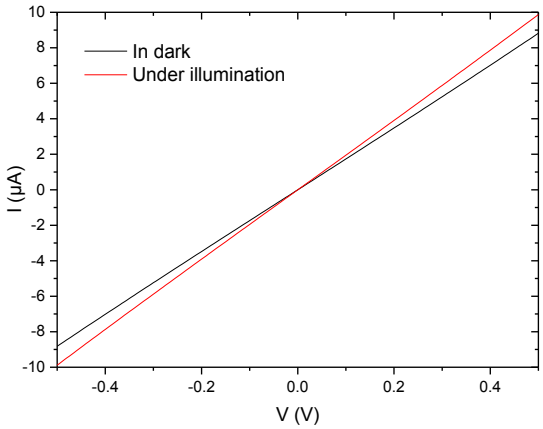

Figure 5. I-V characteristics measured between the two electrodes (drain and source) at V_{DS}=0.5V with and without light exposure (λ = 360 nm and P = 6 μW).

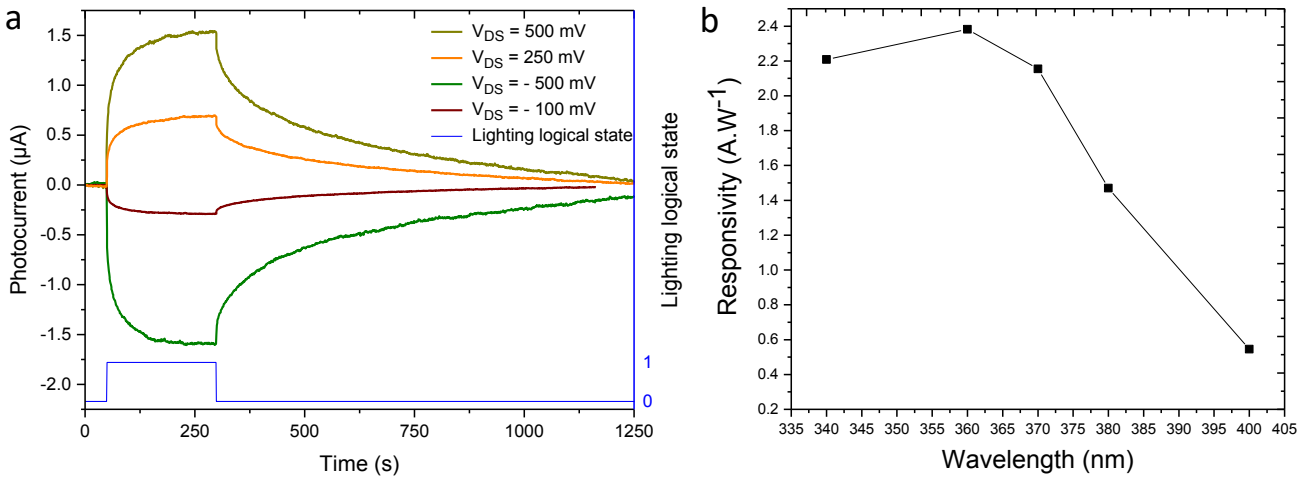

Figure 6. (a) Time responses of the measured photoinduced current at different bias conditions. Under illumination above the GaN band gap the conductance of the graphene measured between the drain-source electrodes increases. The behavior can be described by two regimes; a first rapid increase of the current followed by a saturation. After 250 s of illumination the light is switched off and the relaxation starts with a very slow dynamic. (b) Spectral response of the responsivity of our device near the bandgap of the GaN (λ = 360 nm). Curves are measured at an optical power of about 10 μW·cm^{-2}.

To experimentally observe this sensing mechanism, two Ti/Au electrodes (drain and source) are evaporated onto graphene (the dimension of our device is about 1.5x1.5 mm^2). The current passing through the graphene channel under illumination is then monitored at a constant bias voltage V_{DS} (see Figure 4 showing a schematic representation of our device). An Hg/Xe lamp combined with a monochromator is used as a UV spectroscopic source. The illumination power applied to the samples throughout this work remains with at about 10 μW·cm^{-2}. Figure 5 shows the I-V curves of the device in the dark and under illumination. These curves plot a linear behavior characteristic of this photodetection principle[14]. Indeed the measured current is not flowing through any PN or other semiconductor junction and only measures the graphene resistivity. The difference between the two curves in Figure 5 shows the resistivity change of graphene with and without illumination. The light to charge conversion generates charges trapped in GaN and so modulates the surface charge density of graphene. Then, since graphene is a semimetal, it effectively detects this change and this is how the GaN/graphene photodetector works. Figure 6a shows the response time of the photocurrent ($\Delta I = I_{illumination} - I_{dark}$) growth and decay measured in the graphene at different bias voltage in response to UV illumination being turned on and off. Upon illumination the conductance of the device is enhanced and the relative variation of the current

($\Delta I/I_{dark}$~20%) is bias voltage independent, demonstrating the photogating effect of the GaN islands on graphene.

The shape of the photocurrent responses under illumination seems to show at least two regimes. First, the current of the device rises sharply when illuminated. This increase is then followed by a slower component before saturating. The dynamic response of our device on illumination can be well described by an exponential function with two relaxation times τ_1 and τ_2: $I_{photo} = A \cdot \left(1 - e^{\frac{-t}{\tau_1}}\right) + C \cdot \left(1 - e^{\frac{-t}{\tau_2}}\right)$ where t is the time when UV is switched on or off and A and C are scaling constants. The time constants are estimated from these fits. The shorter relaxation time, $\tau_1 \approx 2\ s$, which illustrates the regime of interest for detection devices, appears to be constant for all experiments. It probably corresponds to the hole transfer from GaN to graphene whereas the slower component ($\tau_2 \sim 50\ s$) may represent the charge transfer within the GaN microstructures. When the light is switched off, photocurrent decay starts. This regime during which the trapped electrons in GaN recombine has a slower dynamic. After a fast part this regime follows an exponential law characterized by a time constant of about 500 s. Such long relaxation times can be drastically reduced by pulsed back-gating[14].

One of the main parameters to quantify the photodetection performances of a device is the responsivity defined as the ratio between the photocurrent and the light beam power ($R = \frac{I_{photo}}{P}$). The curve in Figure 6b shows the spectral response of this parameter in the UV-A range. The recorded current and consequently the responsivity increases clearly when the light wavelength is shorter than the GaN bandgap with a maximum responsivity of 2.5A·W^{-1} at 360 nm and an optical power of about 10 µW·cm^{-2}. In the 340 to 370 nm range the responsivity exceeds 2 A·W^{-1}. It clearly appears that the two materials (GaN and graphene) of our structure play a crucial role in the efficiency of photodetection. GaN is essential in the optical switching process and graphene is used at the same time as a sensitive material and as a substrate for GaN epitaxy to make a self-assembled device. This high responsivity is a clear signature

of the high charge carrier mobility of the graphene base plane after the GaN growth. Photogenerated electrons gets trapped in GaN whereas corresponding holes are transferred to the graphene due to the built in field at the interface (Figure 3). The trapped charges in GaN act as local gate and the holes circulates through graphene to the source electrode thanks to the bias voltage V_{DS}. The current which circulates in graphene is thus modulated by the trapped electrons in GaN. This mechanism can explain the high responsivity measured[14,36,37]. Nevertheless the photodetection efficiency of our device is far from being optimized. The most direct beneficial improvement on both the responsivity and the response time would be a downscaling of our device. Significant improvements (quantum efficiency and speed) also depend on an optimized and well-controlled growth process of GaN islands on graphene, both in terms of density and size to increase UV light absorption in GaN islands near graphene/GaN interface and maximize the numbers of transferred charges towards graphene. The surface over volume ratio of the GaN crystals may be a crucial parameter controlling the surface states that may act as traps for the photogenerated electrons. The GaN surface coverage is also a key parameter because it directly impacts the effective area on which the photogating mechanism occurs. Finally, the detection threshold of the photodetector can even be shifted to deeper UV wavelengths by growing GaN crystals as small as the critical size at which the quantum confinement starts.

Conclusion

Graphene is usually used both as a substrate for GaN epitaxy or as an efficient material for sensing applications. In this article we show that these two functions can be combined to go towards a novel concept of hybrid UV-photodetector based on the direct GaN on graphene assembly. The preservation of the charge carrier mobility within the graphene after the MOCVD process is consequently a key issue. We demonstrate that under specific nucleation conditions graphene withstands the severe atmosphere (chemically aggressive precursors and high temperature) required to get GaN crystals. Under illumination

above the GaN bandgap, the heterostructure exhibits a strong photogating effect with an increase of the photoinduced drain-source current in graphene. The responsivity of our device is in excess of 2 $A \cdot W^{-1}$ in the UV-A range under low illumination conditions (~10 $\mu W \cdot cm^{-2}$). Further improvements of the photodetection performances can be made by downscaling the device and working on a better control of the GaN seeds growth. In comparison with structures using QDs transferred onto graphene, this work opens a route to better control the active interface and the assembly/size distribution of the dots. It will further help to study more precisely the phenomena involved at the interface of hybrid structures mixing graphene with other materials for photodetection. This work has shown the feasibility of making hybrid structures by epitaxy using 2D material as a substrate. As GaN required very aggressive atmosphere to grow, it is reasonable to assume that other traditional semiconductors can also be epitaxially grown while preserving the fascinating properties of the 2D materials.

Experimental section

- **Device Fabrication**

Graphene is grown on Cu foil by chemical vapor deposition (CVD)[19]. It is then transferred onto a sapphire substrate via a wet transfer. Graphene is subsequently annealed to remove the residues that can remain after the transfer process. Prior to the MOCVD growth a second annealing is done to remove the atmospheric pollutants and so to be sure that the graphene is clean. Regarding the growth of GaN microstructures on top of graphene we used a one step process at ~ 950°C on a commercial MOCVD system with a Closed Couple Showerhead (CCS) system. The Ti/Au contact electrodes are made by evaporation using a solid mask.

- **Characterizations**

The morphology study of the GaN microstructures is carried out with a scanning electron microscope (Zeiss FE-SEM Ultra) operating at 1.5 kV. The X-ray diffraction (XRD) is performed with the Cu Kα radiation (on a Panalytical Xpert' setup). Micro-Raman measurements were performed using a 532 nm laser excitation source with an average power of 0.7 μW focused on a ~ 0.5 μm beam diameter (Renishaw InVia setup).

- **Electrical characterizations**

The electrical transport measurements are carried out in a primary vacuum at ambient temperature. The real time DC resistance of the device is recorded using Keithley Source/measure Electrometer 6430 with a bias voltage varying between -0.5 to 0.5 Volts. For the optical response of the device an Hg/Xe lamp combined with a monochromator is used as a UV spectroscopic source.

References

(1) Koppens, F. H. L.; Mueller, T.; Avouris, P.; Ferrari, A. C.; Vitiello, M. S.; Polini, M. Photodetectors Based on Graphene, Other Two-Dimensional Materials and Hybrid Systems. *Nat. Nanotechnol.* **2014**, *9* (10), 780–793.

(2) Bonaccorso, F.; Sun, Z.; Hasan, T.; Ferrari, A. C. Graphene Photonics and Optoelectronics. *Nat. Photonics* **2010**, *4* (9), 611–622.

(3) Park, J.; Ahn, Y. H.; Ruiz-Vargas, C. Imaging of Photocurrent Generation and Collection in Single-Layer Graphene. *Nano Lett.* **2009**, *9* (5), 1742–1746.

(4) Lee, E. J. H.; Balasubramanian, K.; Weitz, R. T.; Burghard, M.; Kern, K. Contact and Edge Effects in Graphene Devices. *Nat. Nanotechnol.* **2008**, *3* (8), 486–490.

(5) Xia, F.; Mueller, T.; Golizadeh-Mojarad, R.; Freitag, M.; Lin, Y.; Tsang, J.; Perebeinos, V.; Avouris, P. Photocurrent Imaging and Efficient Photon Detection in a Graphene Transistor. *Nano Lett.* **2009**, *9* (3), 1039–1044.

(6) Xia, F.; Mueller, T.; Lin, Y.; Valdes-Garcia, A.; Avouris, P. Ultrafast Graphene Photodetector. *Nat. Nanotechnol.* **2009**, *4* (12), 839–843.

(7) Muñoz, E.; Monroy, E.; Pau, J. L.; Calle, F.; Omnès, F.; Gibart, P. III Nitrides and UV Detection. *J. Phys. Condens. Matter* **2001**, *13* (32), 7115.

(8) Zhang, X.; Liu, B.; Liu, Q.; Yang, W.; Xiong, C.; Li, J.; Jiang, X. Ultrasensitive and Highly Selective Photodetections of UV-A Rays Based on Individual Bicrystalline GaN Nanowire. *ACS Appl. Mater. Interfaces* **2017**, *9* (3), 2669–2677.

(9) Zhang, X.; Liu, Q.; Liu, B.; Yang, W.; Li, J.; Niu, P.; Jiang, X. Giant UV Photoresponse of a GaN Nanowire Photodetector through Effective Pt Nanoparticle Coupling. *J. Mater. Chem. C* **2017**, *5* (17), 4319–4326.

(10) Jang, S.; Hwang, E.; Lee, Y.; Lee, S.; Cho, J. H. Multifunctional Graphene Optoelectronic Devices Capable of Detecting and Storing Photonic Signals. *Nano Lett.* **2015**, *15* (4), 2542–2547.

(11) Guo, W.; Xu, S.; Wu, Z.; Wang, N.; Loy, M. M. T.; Du, S. Oxygen-Assisted Charge Transfer Between ZnO Quantum Dots and Graphene. *Small* **2013**, *9* (18), 3031–3036.

(12) Lu, Y.; Wu, Z.; Xu, W.; Lin, S. ZnO Quantum Dot-Doped Graphene/h-BN/GaN-Heterostructure Ultraviolet Photodetector with Extremely High Responsivity. *Nanotechnology* **2016**, *27* (48), 48LT03.

(13) Sun, Z.; Liu, Z.; Li, J.; Tai, G.; Lau, S.-P.; Yan, F. Infrared Photodetectors Based on CVD-Grown Graphene and PbS Quantum Dots with Ultrahigh Responsivity. *Adv. Mater.* **2012**, *24* (43), 5878–5883.

(14) Konstantatos, G.; Badioli, M.; Gaudreau, L.; Osmond, J.; Bernechea, M.; de Arquer, F. P. G.; Gatti, F.; Koppens, F. H. L. Hybrid Graphene-Quantum Dot Phototransistors with Ultrahigh Gain. *Nat. Nanotechnol.* **2012**, *7* (6), 363–368.

(15) Kumaresan, V.; Largeau, L.; Madouri, A.; Glas, F.; Zhang, H.; Oehler, F.; Cavanna, A.; Babichev, A.; Travers, L.; Gogneau, N.; Tchernycheva, M.; Harmand, J.-C. Epitaxy of GaN Nanowires on Graphene. *Nano Lett.* **2016**, *16* (8), 4895–4902.

(16) Heilmann, M.; Sarau, G.; Göbelt, M.; Latzel, M.; Sadhujan, S.; Tessarek, C.; Christiansen, S. Growth of GaN Micro- and Nanorods on Graphene-Covered Sapphire: Enabling Conductivity to Semiconductor Nanostructures on Insulating Substrates. *Cryst. Growth Des.* **2015**, *15* (5), 2079–2086.

(17) Kang, S.; Mandal, A.; Chu, J. H.; Park, J.-H.; Kwon, S.-Y.; Lee, C.-R. Ultraviolet Photoconductive Devices with an N-GaN Nanorod-Graphene Hybrid Structure Synthesized by Metal-Organic Chemical Vapor Deposition. *Sci. Rep.* **2015**, *5*, 10800.

(18) Kim, J.; Bayram, C.; Park, H.; Cheng, C.-W.; Dimitrakopoulos, C.; Ott, J. A.; Reuter, K. B.; Bedell, S. W.; Sadana, D. K. Principle of Direct van Der Waals Epitaxy of Single-Crystalline Films on Epitaxial Graphene. *Nat. Commun.* **2014**, *5*, 4836.
(19) Han, Z.; Kimouche, A.; Kalita, D.; Allain, A.; Arjmandi-Tash, H.; Reserbat-Plantey, A.; Marty, L.; Pairis, S.; Reita, V.; Bendiab, N.; Coraux, J.; Bouchiat, V. Homogeneous Optical and Electronic Properties of Graphene Due to the Suppression of Multilayer Patches During CVD on Copper Foils. *Adv. Funct. Mater.* **2014**, *24* (7), 964–970.
(20) Gibart, P. Metal Organic Vapour Phase Epitaxy of GaN and Lateral Overgrowth. *Rep. Prog. Phys.* **2004**, *67* (5), 667.
(21) Amano, H.; Sawaki, N.; Akasaki, I.; Toyoda, Y. Metalorganic Vapor Phase Epitaxial Growth of a High Quality GaN Film Using an AlN Buffer Layer. *Appl. Phys. Lett.* **1986**, *48* (5), 353–355.
(22) Wang, S.; Zhang, Y.; Abidi, N.; Cabrales, L. Wettability and Surface Free Energy of Graphene Films. *Langmuir* **2009**, *25* (18), 11078–11081.
(23) Dobrovinskaya, E. R.; Lytvynov, L. A.; Pishchik, V. Properties of Sapphire. In *Sapphire*; Micro- and Opto-Electronic Materials, Structures, and Systems; Springer US, 2009; pp 55–176.
(24) Nakada, K.; Ishii, A. Migration of Adatom Adsorption on Graphene Using DFT Calculation. *Solid State Commun.* **2011**, *151* (1), 13–16.
(25) Kim, Y.; Cruz, S. S.; Lee, K.; Alawode, B. O.; Choi, C.; Song, Y.; Johnson, J. M.; Heidelberger, C.; Kong, W.; Choi, S.; Qiao, K.; Almansouri, I.; Fitzgerlad, E. A.; Kong, J.; Kolpak, A. M.; Hwang, J.; Kim, J. Remote Epitaxy through Graphene Enables Two-Dimensional Material-Based Layer Transfer. *Nature* **2017**, *544* (7650), 340–343.
(26) Couto, N. J. G.; Costanzo, D.; Engels, S.; Ki, D.-K.; Watanabe, K.; Taniguchi, T.; Stampfer, C.; Guinea, F.; Morpurgo, A. F. Random Strain Fluctuations as Dominant Disorder Source for High-Quality On-Substrate Graphene Devices. *Phys. Rev. X* **2014**, *4* (4), 041019.
(27) Lee, J. E.; Ahn, G.; Shim, J.; Lee, Y. S.; Ryu, S. Optical Separation of Mechanical Strain from Charge Doping in Graphene. *Nat. Commun.* **2012**, *3*, 1024.
(28) Froehlicher, G.; Berciaud, S. Raman Spectroscopy of Electrochemically Gated Graphene Transistors: Geometrical Capacitance, Electron-Phonon, Electron-Electron, and Electron-Defect Scattering. *Phys. Rev. B* **2015**, *91* (20), 205413.
(29) Banszerus, L.; Janssen, H.; Otto, M.; Epping, A.; Taniguchi, T.; Watanabe, K.; Beschoten, B.; Neumaier, D.; Stampfer, C. Identifying Suitable Substrates for High-Quality Graphene-Based Heterostructures. *2D Mater.* **2017**, *4* (2), 025030.
(30) Das, A.; Pisana, S.; Chakraborty, B.; Piscanec, S.; Saha, S. K.; Waghmare, U. V.; Novoselov, K. S.; Krishnamurthy, H. R.; Geim, A. K.; Ferrari, A. C.; Sood, A. K. Monitoring Dopants by Raman Scattering in an Electrochemically Top-Gated Graphene Transistor. *Nat. Nanotechnol.* **2008**, *3* (4), 210–215.
(31) Romero, H. E.; Joshi, P.; Gupta, A. K.; Gutierrez, H. R.; Cole, M. W.; Tadigadapa, S. A.; Eklund, P. C. Adsorption of Ammonia on Graphene. *Nanotechnology* **2009**, *20* (24), 245501.
(32) Lin, Y.-C.; Lin, C.-Y.; Chiu, P.-W. Controllable Graphene N-Doping with Ammonia Plasma. *Appl. Phys. Lett.* **2010**, *96* (13), 133110.
(33) Yan. Determination of Graphene Work Function and Graphene-Insulator-Semiconductor Band Alignment by Internal Photoemission Spectroscopy. *Appl. Phys. Lett.* **2012**, *101* (2), 022105.
(34) Yu, Y.-J.; Zhao, Y.; Ryu, S.; Brus, L. E.; Kim, K. S.; Kim, P. Tuning the Graphene Work Function by Electric Field Effect. *Nano Lett.* **2009**, *9* (10), 3430–3434.
(35) Zhang, Y.; Tan, Y.-W.; Stormer, H. L.; Kim, P. Experimental Observation of the Quantum Hall Effect and Berry's Phase in Graphene. *Nature* **2005**, *438* (7065), 201–204.
(36) Guo, Q.; Pospischil, A.; Bhuiyan, M.; Jiang, H.; Tian, H.; Farmer, D.; Deng, B.; Li, C.; Han, S.-J.; Wang, H.; Xia, Q.; Ma, T.-P.; Mueller, T.; Xia, F. Black Phosphorus Mid-Infrared Photodetectors with High Gain. *Nano Lett.* **2016**, *16* (7), 4648–4655.

(37) Furchi, M. M.; Polyushkin, D. K.; Pospischil, A.; Mueller, T. Mechanisms of Photoconductivity in Atomically Thin MoS2. *Nano Lett.* **2014**, *14* (11), 6165–6170.

TOC